LANGMUIR Article
Cite This: Langmuir 2019, 35, 15552−15563
pubs.acs.org/Langmuir

Interaction Profiles and Stability of Rigid and Polymer-Tethered Lipid Bilayer Models at Highly Charged and Highly Adhesive Contacts

Pierluigi Bilotto,[†,∥] Maximilian Lengauer,[†,∥] Jakob Andersson,[‡] Ulrich Ramach,[†,§] Laura L. E. Mears,[†] and Markus Valtiner*[,†]

[†]Institute of Applied Physics, Vienna University of Technology, Vienna 1040, Austria
[‡]Austrian Institute of Technology, Vienna 1210, Austria
[§]CEST Kompetenzzentrum für elektrochemische Oberflächentechnologie, Wiener Neustadt 2700, Austria

Supporting Information

ABSTRACT: Understanding interaction force versus distance profiles of supported lipid bilayers (SLBs) is relevant to a number of areas, which rely on these model systems, including, e.g., characterization of ligand/receptor interactions or bacterial adhesion. Here, the stability of 4 different SLB architectures was compared using the surface forces apparatus (SFA) and atomic force microscopy (AFM). Specifically, the outer envelope of the bilayer systems remained constant as 1,2-dipalmitoyl-*sn*-glycero-3-phosphocholine (DPPC). The inner layer was varied between DPPC and 1,2-dipalmitoyl-3-trimethylammonium-propane (DPTAP) both on mica, and self-assembled monolayers (SAMs) of hexadecanethiol and the polymer-tethered diphytanylglycerol-tetraethylene glycol-lipoid acid (DPhyTL) on smooth gold surfaces. In that same order these gave an increasing strength of interaction between the inner layer and the supporting substrate and hence improved stability under highly adhesive conditions. Detachment profiles from highly charged and highly adhesive contacts were characterized, and approach characteristics were fitted to DLVO models. We find increasing stability under highly adhesive loads, approaching the hydrophobic limit of the adhesive energy between the inner and outer layers for the SAM-based systems. For all four SLBs we further compare AFM surface topographies, which strongly depend on preparation conditions, and the DLVO fitting of the SFA approach curves finds a strong charge regulation behavior during interaction, dependent on the particular model system. In addition, we find undulation characteristics during approach and separation. The increased stability of the complex architectures on a gold support makes these model systems an ideal starting point for studying more complex strongly adhesive/interacting systems, including, for example, ligand/receptor interactions, biosensing interactions, or cell/surface interactions.

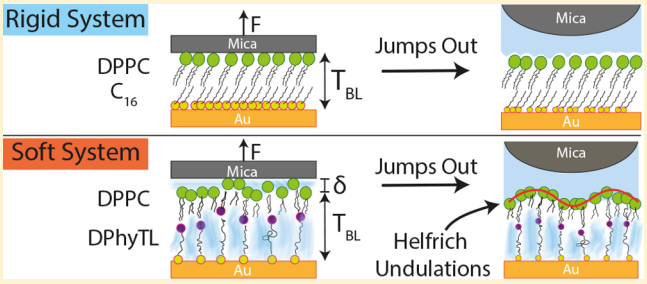

INTRODUCTION

Biophysical interactions on cell membranes can be well-modeled experimentally using supported lipid bilayers (SLBs) as an excellent system for mimicking complex cell membranes. SLBs are particularly useful for characterizing membrane/membrane, membrane/substrate, or ligand/receptor interactions in biomimetic systems. For example, SLBs can be used to build up biosensing devices based on ligand/receptor interactions,[1] or they can mimic cell/cell interaction processes.[2−4] Specifically the surface forces apparatus (SFA) has been established as a unique tool for lipid bilayer experiments to measure force versus distance characteristics during approach and separation of lipid bilayers, e.g., for quantifying ligand/receptor interactions, bilayer fusion and hemifusion, or intercellular adhesion.[3−9] Alternatively SLBs can be used as a supporting system for polymers enabling the formation of mushroom and brush regimes with controlled density and functionality,[10−12] allowing fundamental interactions between functional groups and surfaces to be probed with the SFA.

In all applications the stability of an SLB system is central, and force probe experiments provide a detailed insight into the stability of SLBs. In a 1,2-dipalmitoyl-*sn*-glycero-3-phosphocholine (DPPC) bilayer versus DPPC bilayer contact, the stability has been measured using SFA by Orozco-Alcarez and Kuhl,[8] finding a work of adhesion proportional to 0.5 mJ/m^2. Benz et al.[13] used a combination of SFA and AFM on a bilayer versus bilayer system with DLPE/DPPE as the outer and inner layers, respectively. For their most densely packed or "saturated" bilayers, repeated force−distance measurements

Special Issue: Intermolecular Forces and Interfacial Science

Received: June 25, 2019
Revised: August 30, 2019
Published: September 1, 2019

DOI: 10.1021/acs.langmuir.9b01942
Langmuir 2019, 35, 15552−15563

consistently reached the same hard wall contact bilayer thickness, even at pressures over 100 MPa. A similar work of adhesion compared to the DPPC−DPPC contact, $W \approx 0.5$ mJ/m^2, was found. In contrast, when holes in one or both layers were present in the SLB and identified in AFM, with increased applied force the two bilayers' structure broke down, and hemifusion of the layers occurred (and hence an adhesive, JKR contact) even if initially a nonadhesive (Hertzian) contact was found. The adhesion values increased dramatically into the high-adhesion regime, between 15 and 21 mJ/m^2 for the 18−30% defect area.

In this work we are interested in two aspects of SLB systems. First, we aim to develop a lipid bilayer model system for SFA that is defect-free (e.g., no holes) and stable under electrochemical conditions, offering the future possibility to charge/discharge membranes during interaction force measurements, or *vice versa* to measure charge and discharge during interaction. In this direction, SLB systems already established for biosensing devices are an ideal starting point.[14] Second, we aim to improve SLB stability under highly adhesive conditions, which are to be expected not only in electrochemical systems but also in certain cell processes. In this work, we define high adhesion to be values above ∼15 mJ/m^2 as these are the values that occur for processes, such as hemifusion of bilayers, and hence are biologically significant for understanding events like membrane fusion.[2,7] The interaction between a single lipid bilayer on one side and a solid surface without modifications on the other is less commonly investigated[15,16] but provides a simple experimental system where the contact is likely to be highly adhesive and where stability can be tested under extreme conditions. Two investigations of such an SLB against a hydrophilic surface, silica and mica, respectively, have been made experimentally by Anderson et al.,[15] and using Grand Canonical Monte Carlo (GCMC) simulations by Pertsin and Grunze,,[16] with different conclusions. In the experimental measurements, in water only a repulsive force was observed during the approach of silica to the SLB on mica. However, the simulations predict that as the separating distance decreases there is an attractive force between mica and the SLB leading to a jump into contact. Within the simulations, undulations and spontaneous protrusions of molecules from the SLB were observed. It is unclear whether differences in surface topography, lipid headgroup, or surface material should result in such changes in the force profiles from the two different approaches.

Here, we discuss force profiles of different SLB models facing an atomically smooth mica surface (see Figure 1) in the context of the theoretical work of Pertsin and Grunze[16] and the experimental data of Anderson with SLBs facing silica.[15] Further, we compare the stability of classic solid-supported bilayer model systems with two alternative support methods based on self-assembly chemistry on gold for the inner leaflet of an SLB (see again Figure 1). Specifically, we compare the classic inner layer anchoring on silica-based materials (e.g., mica or glass) via (1) uncharged lipids with (2) anchoring via a positively charged lipid, and anchoring via two electrochemically polarizable systems including (3) a rigid and hydrophobic linear hexadecanethiol self-assembled monolayer (SAM) as well as (4) a flexible SAM-anchored and polymer-tethered lipid layer, diphytanylglycerol-tetraethylene glycol-lipoid acid, better known as DPhyTL.

We apply similar methods to Benz et al.[13] to test the stability of SLBs contacting a highly charged and adhesive solid surface,

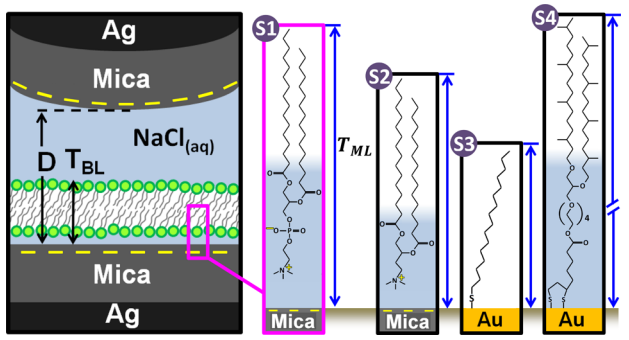

Figure 1. SFA configuration and chemical structures of the inner layers. The SFA configuration is shown for system S1. The bilayer system was placed on one side, and a blank mica surface was used as the apposing surface. All samples were immersed in 8 mM NaCl. The silver layers form the interferometric cavity. The distance D and the bilayer thickness T_{BL} are defined in the schematic. Chemical structures of the inner layers. System S1, DPPC/DPPC on mica; System S2, DPPC/DPTAP on mica; System S3, DPPC/hexadecanethiol on Au; System S4, DPPC/DPhyTL on Au.[23] T_{ML} indicates the monolayer thickness.

namely, mica. Specifically, we compare AFM surface topographies and force versus distance characteristics using the SFA. We find undulation forces and charge regulation during interaction, which strongly depend on preparation conditions and the particular model system, respectively. We also find an increased long-term stability under highly adhesive conditions and ideal electrochemical characteristics of a biomembrane for the DPhyTL system, making this model system for SFA an ideal starting point for studying more complex strongly adhesive/interacting systems. For instance, DPhyTL has been extensively used in other fields to assemble various model membrane architectures that have been applied to the study of bacterial toxins such as Gramicidin,[17] α-hemolysin,[18] and valinomycin[19] and the interaction of silver nanoparticles with cellular membranes[20] and to mimic the outer membrane of Gram-negative bacteria.[21] DPhyTL-anchored membranes also show long-term stability for biosensing measurements, stable in the range of months.[22]

EXPERIMENTAL SECTION

Materials. The lipids used in this work were 1,2-dipalmitoyl-*sn*-glycero-3-phosphocholine (DPPC) and 1,2-dipalmitoyl-3-trimethylammonium-propane (DPTAP), purchased from Avanti Polar Lipids. The lipids were dissolved in pure chloroform from Carl Roth (assay: ≥99.9%), with lipid mass concentrations of 1 mg/mL for DPPC and 0.25 mg/mL for DPTAP.

The other chemicals/materials were sourced as follows: muscovite mica [S&J Trading (elastic modulus 90−180 GPa)[24,25]], sodium chloride from Carl Roth (assay: ≥99%), *n*-hexane from Carl Roth (assay: ≥98%), ethanol ≥99.9% pure from VWR, hexadecanthiol (C_{16}−SH, assay: 99%) from Sigma-Aldrich, Inc., diphytanylglycerol-tetraethylene glycol-lipoid acid (DPhyTL) from Celestial Synthetics, EPO-TEK heat curable glue (EPO-TEK 377) from Epoxy Technology (elastic modulus 2.58 GPa), and UV curable glue (NOA 81) from Norland Products Inc. (elastic modulus 1.38 GPa). Milli-Q water (Milli-pore, TOC value <2 ppb, resistivity >18 MΩ) was used throughout.

Assessment of Water Quality. Inductively coupled plasma mass spectrometry (ICP-MS) is used periodically in our lab to check water quality (see Table S1 in the Supporting Information for the typical and most abundant contaminants in Milli-Q water, and solutions prepared from Milli-Q water). The base level ionic strength of standard Milli-Q water is at 5 × 10^{-6} mol/L; subsequent distillation

DOI: 10.1021/acs.langmuir.9b01942
Langmuir 2019, 35, 15552−15563

can lower this base level by more than 1 order of magnitude to 1×10^{-6} mol/L. Upon addition of 10 mM of salt the background contribution to the ionic strength increases by an additional 5×10^{-5} and 2×10^{-5} mol/L if glass or plastic bottles are used due to contaminants added from the salt and the glass, respectively. We typically work with standard Milli-Q water mixed in plastic bottles, placing our background level to a total of 7×10^{-5} mol/L.

Supported Lipid Bilayers (SLBs). *Langmuir–Blodgett Deposition of SLBs.* A Langmuir–Blodgett (LB) trough, built by Dr. Hans Riegler (Max-Planck Institute for Colloid and Interface Research, Potsdam), with a deep central well for sample transfer was used for the LB measurements and depositions. The LabView written control software for processing the signals from the barrier motor and from the Wilhelmy plate was kindly provided by Dr. Michael Kappl from the Max Planck Institute for Polymer Research. Our studies with the LB trough were carried out with lipid amounts of 0.46–1.09 μMol. For DPPC/DPTAP mixtures, the defined volumes of lipid containing solutions were dropped onto the water surface successively. Mixture molar ratios (DPPC:DPTAP) applied were 37:63, 47:53, and 81:19. At least 4 independent surface pressure–area isotherms were measured for each mixture to obtain the respective lipid area per molecule at a surface pressure of $\Pi = 42$ mN/m (Figure S1). Those gave, together with the defined mixture ratios, a direct relation to the charge densities of the lipid monolayers.

For depositing lipid layers onto substrates, the Langmuir–Blodgett method was applied; i.e., the substrate was moved vertically with 15 μm/s through the lipid monolayer (out of/into bulk water for inner/outer layer deposition), at a preadjusted surface pressure of $\Pi = 42$ mN/m. Hence, the outer lipid layer deposition ended with the sample fully submerged under water, ready for underwater transfer to the relevant measurement cell.

SAM-Based Systems. We prepared the two different SAM-based systems as follows. The hexadecanethiol (C_{16}–SH) was deposited by immersion in a 1 mM solution in pure filtered ethanol (0.2 μm pore size) onto a smooth gold film substrate nominally 40 nm thick (template striped from atomically smooth mica; see the Surface Forces Apparatus section for deposition method) glued to a cylindrical or flat disk depending on whether it was for an SFA or AFM experiment. We kept the substrate in solution for 1 h in the dark and at constant room temperature. After deposition, the substrate was sonicated consecutively in pure *n*-hexane and pure filtered ethanol. For the DPhyTL deposition a 0.1 mg/mL DPhyTL solution was prepared in pure ethanol and into which the gold substrate was immersed following the same protocol as described for the C_{16} deposition. The outer layer of our sample was always DPPC, deposited as a monolayer with the Langmuir–Blodgett technique described above, with the sample ending inside the trough.

Atomic Force Microscopy. The atomic force microscopy was performed with an Asylum Research Cypher ES atomic force microscope (Oxford Instruments) in amplitude modulation mode (AM-AFM). All samples were imaged in 8 ± 1 mM NaCl solution. In liquid environments, cantilevers with a given resonance frequency of 2000 kHz (Nanosensors, product name: Arrow UHFAuD) were used. For measuring in air, silicon cantilevers with a resonance frequency of about 330 kHz (Nanosensors, product name: PPP-NCHAuD) were applied. For both cantilever types the back side was gold-coated for photothermal excitation (blueDrive mode). For data processing and analysis of the topography data, the Asylum software package was used. For image leveling, second-order polynomial fitting was applied. For each SLB system, at least 3 independent AFM measurements were carried out.

Surface Forces Apparatus. Two different surface forces apparatus (SFA) were used for normal force measurements in transmission mode. The first one is the SFA 2000 (SurForce LLC, Santa Barbara, CA) utilized to perform the experiments on lipid-bilayers deposited on mica. The second one is a new SFA prototype developed in our laboratories. It introduces advantages in terms of the optics, alignment, and sample handling during the experiment.[26] Semiconductor strain gauges can also be included on the spring to allow simultaneous force measurements, independent from the optical measurement. Mica sheets used in these experiments were hand-cleaved to provide sheets with an area of 5–10 cm^2 and uniform thickness raging from 3 to 5 μm. The edges of these sheets were melt-cut with a hot platinum wire. Using a PVD with a base pressure of 5×10^{-7} mbar by BestTec (Berlin, Germany) the mica sheets were back-silvered by electron beam deposition or by thermal deposition (Auto306 Lab Coater, HHV, Crawley, UK) with nominal 40 nm thickness.

To perform the experiments with SLBs, the sheets were glued on cylindrical fused silica disks with a nominal radius of curvature $R = 1$–2 cm using a UV-curable glue. In the case of SAM-based experiments, the substrates consisted of atomically smooth gold films (described in SAM-based systems above). As in previous work, initially, substrates were glued with NOA81 (Norland adhesives, UV-curable adhesive); however, significant plastic deformation of the surface occurred during SFA experiments under highly adhesive load (contact deformation is shown in the SI, Figure S2). EPO-TEK 377 (Epotek Technologies Inc.), a heat-cured glue, was identified and used (if not otherwise specified) as a harder alternative and showed improvements to the smoothness of the gold in AFM (see the SI, Figure S3A,B) and did not deform under highly adhesive loads. All measurements were performed in 8 ± 1 mM NaCl. For each system investigated, a minimum of two completely independent and quantitatively similar SFA experiments were performed with a minimum of three force curves recorded on at least two individual contact points. Further details on the SFA technique are given in previous works.[26,27]

The SFA data analysis was performed with SFA Explorer, a program developed in our laboratories that uses the multiple matrix method to simulate the multiple beam interferometry taking place in the SFA optical cavity, translating the measured spectra from the fringes of equal chromatic order (FECO) into absolute distances between the surfaces with uncertainty equal to 0.05 nm, and lateral resolution of 1.56 μm per pixel.[26]

RESULTS AND DISCUSSION

In this work we characterize the four different supported lipid bilayer (SLB) model systems, which have distinctly different innerlayer anchoring chemistry (S1–S4), as shown in Figure 1. We test the force response for all model systems against a highly charged surface, as well as their stability upon de-adhesion from highly adhesive contacts. Topography and undulations of the bilayers were characterized with AFM imaging, and force distance profiles during approach and separation (de-adhesion) were recorded using the SFA.

Figure 2 shows the force versus distance characteristics recorded during approach of mica to the DPPC/DPPC system supported on a mica surface (labeled S1) for two consecutive profiles. In the first approach, when the surfaces touch for the first time, a long-range electric double layer repulsion is followed by a jump to a distance $T_{BL} = 4.3 \pm 0.5$ nm corresponding to the DPPC bilayer thickness.[28] With increasing external force the bilayer is compressed, and the mica to mica distance reaches a minimum value of $D = 1.1 \pm 0.2$ nm at $F/R = 30$ mN/m. This indicates that the bilayer does not maintain a stable thickness upon compression, which suggests an unstable bilayer under very moderate compression.

A further indication of instability of the S1 system is that, in the second approach, a jump-in to $T^*_{BL} = 9.7 \pm 0.5$ nm occurred, which is about double the distance compared to the first force measurement. Also during the second approach increasing load resulted in a considerable compression of the confined material. This is not surprising and indicates that the bilayer was considerably damaged during the first separation. The molecular mechanism is depicted in the sketch of Figure 2 as follows: (i) When the system has been compressed for the first time the bilayer is sandwiched between the two identical

DOI: 10.1021/acs.langmuir.9b01942
Langmuir 2019, 35, 15552–15563

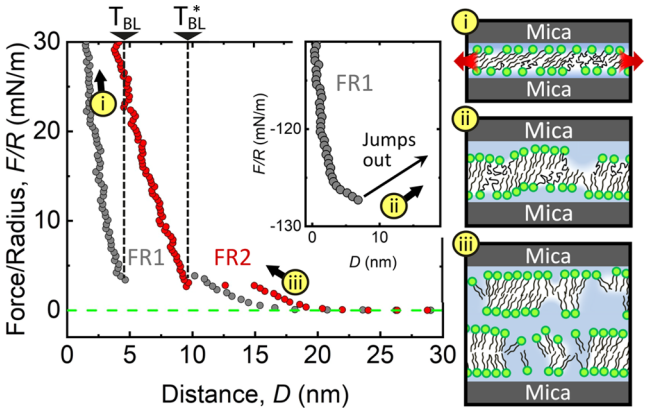

Figure 2. DPPC/DPPC bilayer (S1) LB-deposited on muscovite mica. Force−distance profile of the approaches from two sequential force runs of S1 in electrolyte NaCl solution (λ_D = 3.57 nm). The first is denoted FR1 (gray), and the second is FR2 (red). After the first profile jumps to a distance $D = T_{BL}$, representing the bilayer thickness in confinement, (i) the surfaces are in contact, and a compressing force F_C is applied to the system, squeezing the bilayer. When the surfaces are moved apart, the bilayer adheres to both mica sheets, and an equal adhesion force, F_{adh}, acts at both interfaces. When the surfaces jump out of contact, (ii) the bilayer bridges the gap during separation before breaking, and (iii) parts of the bilayer remain on both sides. As a consequence, the force profile is shifted to higher distances for FR2, and a jump-in to a distance $D = T^*_{BL}$ is observed, which has approximately double the value of T_{BL}.

mica surfaces, with equal surface attraction to both sides of the bilayer. (ii) Due to the symmetry of the system (similar interaction of lipid head groups with both confining surfaces), during the jump-out it is likely that parts of the bilayer have remained in contact with the apposing mica surface, as indicated by the U-shaped force versus distance characteristic during separation with a jump out of contact at about D = 8 nm, almost twice the T_{BL} (inset in Figure 2). (iii) When the surfaces are then brought out of contact again, some lipids will remain attached to each of the two surfaces, i.e., some transfers from the original surface to the apposing one due to similar interaction strength with either side. For this reason, when the surfaces are brought together for a second time, the configuration will be similar to two bilayer island covered substrates interacting with each other, consequently jumping into an initial contact at a distance that is double the expected bilayer thickness.

It is possible to overcome this issue by choosing anchoring lipids with a stronger interaction to the mica surface. A frequent choice for SFA experiments has been other zwitterionic lipids with a phosphatidylethanolamine (PE) termination to improve stability, relying on the strong interaction of the terminal primary amine of the PE group with mica.[13,29]

In the following we will show results of similar measurements with three different anchoring mechanisms, including a positively charged lipid (DPTAP), which will work in a similar way compared to PE, with its charge providing additional interaction with the negative mica surface. Additionally we also tested two self-assembled monolayers (SAMs) that have been used to modify surfaces for SLBs used in biosensing and other fields.[14,30] Although these SAM-based systems do not follow the classical definition of an SLB, as only the outer leaflet is composed of lipid molecules, SLB will be used throughout for simplicity.

AFM Topography of Bilayer Models. We first inspected all of the different architectures (labeled S1−S4, according to the anchoring) using AFM topography imaging as displayed in Figure 3. The sketches above represent our interpretations of the scan images.

The topography of S1 (Figure 3A) contained multiple round-shaped defects with a typical diameter of 600 nm, a typical coverage of 20%, and depths between 3.65 and 5.25 nm. Such defect structures are well-known for similar SLB systems and were shown to represent the thermodynamically equilibrated structure of the membrane at a constant temperature,[13] and similar defects were observed for similar SLBs by Hui et al. using AFM.[31]

In contrast, as shown in Figure 3B the surface topography of the mica-supported DPPC/DPTAP system (S2, see again Figure 1) showed no bilayer defects but a division in bilayer regions with clear boundaries and a distinct height difference of typically 0.4 nm. This was observed in all AFM measurements on S2 and over several hours of measuring, which indicates a phase coexistence. There are three ways we suggest that this coexistence could have occurred: the first, most likely cause is heating of the sample by the laser; the sample holder was found to be warm to the touch following measurements;[32] second, charge may lead to more ions present at the mica/DPTAP interface which are trapped beneath the bilayer causing undulations. Lastly, there could be flip-over of lipids between the inner and outer leaflet, which may adjust the transition temperature.

Using a charged lipid (here, DPTAP) as the anchoring lipid maximizes the electrostatic lipid−substrate attraction. For a gel-phase DPTAP film, i.e., the highest possible compression and hence charge per area, pressure isotherms at the water−air interface (see the SI, Figure S1A,B, which are comparable to the literature[33]) indicate that the mica surface charge can be theoretically compensated by up to 95%, considering an ideal mica. Therefore, as it is higher in electrostatic attraction it serves as a benchmark for increasing the stability via charge compensation. The absence of holes or other large-scale defects in S2 aligns with the additional electrostatic attraction to the mica substrate.

To increase the binding energy between the SLB and the substrate, we further introduced two hydrophobic self-assembled monolayer (SAM) systems, that are covalently bound to the gold support, which also offers the future possibility to polarize the membrane in an electrochemical SFA.[34,35]

First, hexadecanethiol was applied as a hydrophobic anchoring layer (i.e., inner layer of S3), as shown in Figure 1. This provides a uniform inner layer with high molecular packing density. An AFM scan image of S3 is shown in Figure 3C. The root-mean-square roughness of about RMS = 0.2 nm demonstrates the absence of defects in the system and a very flat surface topography. These undulations left in the system are shown to be situated in the bilayer itself, rather than within the inner, SAM layer underneath or the gold substrate layer which are defect-free (see the SI, Figure S3B, for gold for direct comparison). No phase coexistence was observed on these layers, possibly due to the limited fluidity of the outer layer on this support, or due to other effects such as slightly different tilt angles imposed by the SAM which may in turn shift phase equilibria.

DOI: 10.1021/acs.langmuir.9b01942
Langmuir 2019, 35, 15552−15563

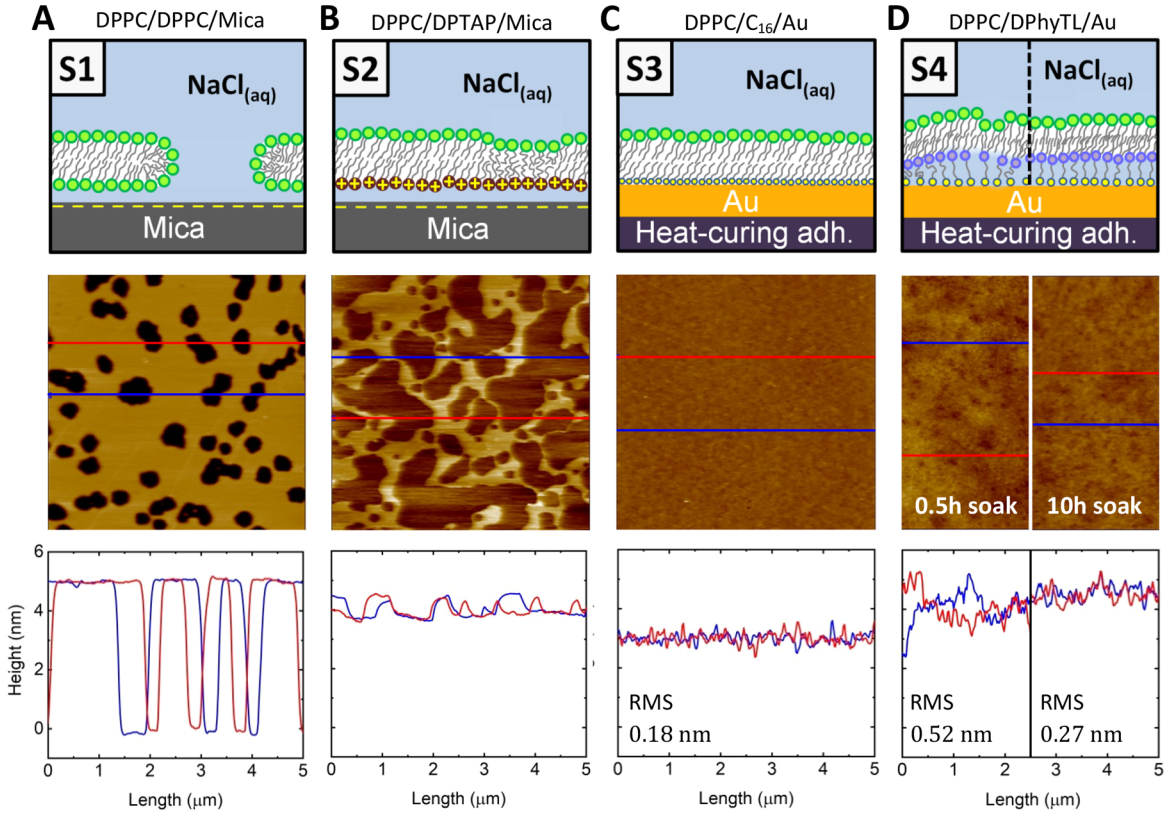

Figure 3. AFM scan images of the lipid bilayer systems investigated. Two height profiles are given below the images to represent the whole system. (A) System S1: mica-supported DPPC bilayer. Here, the height difference of the round-shaped defects is 5.15 ± 0.03 nm. (B) System S2: mica-supported DPPC/DPTAP bilayer. The height difference of the distinct regions is 0.40 ± 0.03 nm. (C) System S3: DPPC/hexadecanethiol bilayer on a gold substrate, prepared with EPO-TEK 377. (D) System S4: DPPC/DPhyTL bilayer on a gold substrate, prepared with EPO-TEK 377. Left: DPPC deposition immediately after SAM generation, further denoted as the not fully hydrated system S4. Right: 10 h storage of the SAM in Milli-Q water before DPPC deposition, further denoted as the fully hydrated system S4. The given RMS values for C and D were calculated from the line profiles shown. The sketches above show our interpretation of the obtained surface topographies.

The second SAM system applied was DPhyTL as the anchoring layer (S4), which has a gold-binding disulfide group linked to a highly branched phytanyl lipid by a hydrophilic tetraethyleneglycol (PEG4) polymer chain (see again Figure 1). The surface topography of system S4, revealed by AFM, strongly depended on the storage time of the DPhyTL in water (Milli-Q). Immediate DPPC deposition after SAM generation and subsequent measurement gave a moderate coverage of large-scale undulations of the bilayer, resulting in a comparably higher RMS value of about 0.5 nm (Figure 3D, left). These undulations level-out considerably with extended immersion times in Milli-Q water for both an exposed DPhyTL monolayer and a fully formed SLB on DPhyTL (Figure 3D, right). The origin of these undulations is located in the flexible anchoring layer, which is clear from our AFM measurements on the DPhyTL monolayer in aqueous solution (see the SI, Figure S3C), showing the same undulating structures of the SAM. In addition, the gold substrate (see the SI, Figure S3B) exhibits a negligible roughness of RMS = 0.05 nm. System S4 further shows randomly arranged defect structures of less than 1 nm depth, which appear to become smaller in size but remain visible with extended immersion time of the monolayer in Milli-Q water. These local defects were not observed in the DPhyTL monolayer (see the SI, Figure S3C) and are hence consistent with a phase coexistence in the outer DPPC layer.

The comparison of the topography of system S4 for different immersion times in Milli-Q water indicates that the PEG4-chain tether, which is buried under the highly branched lipid, needs an extended hydration time to reach an equilibrium of the system with the aqueous environment. A 10 h immersion time of the SAM before DPPC deposition was shown to be sufficient for leveling out the long-range undulations and is further denoted as the fully hydrated system S4.

Interaction Force Profiles of SAM-Based Bilayers. Comparing the two SAM-based systems, S3 clearly gives a higher-quality surface topography. While S4 has more undulations, bringing it closer to natural membranes, the PEG rehydration requires extended exposure to Milli-Q water (about 10 h is sufficient for full PEG hydration). All systems S2, S3, and S4 show promising topography for providing a stable bilayer during force probe experiments and specifically under high adhesion. Here, we will now asses this by direct force probe experiments using the SFA. Figure 4 shows the force versus distance characteristics of S3 and S4 approaching a mica surface recorded with the SFA. Briefly, measurements for S2 (not shown) facing a mica surface also demonstrated instability under high adhesion, with no consistent thickness and adhesion reached over multiple measurements at the same contact. Results were qualitatively comparable but less severe compared to S1 shown in Figure 2.

Figure 4A displays the force versus distance characteristic for S3 facing a mica surface (see the top right inset of Figure 4A). First, the force profiles indicate a long-range electric double layer repulsion scaling with the Debye length, a jump into

DOI: 10.1021/acs.langmuir.9b01942
Langmuir 2019, 35, 15552−15563

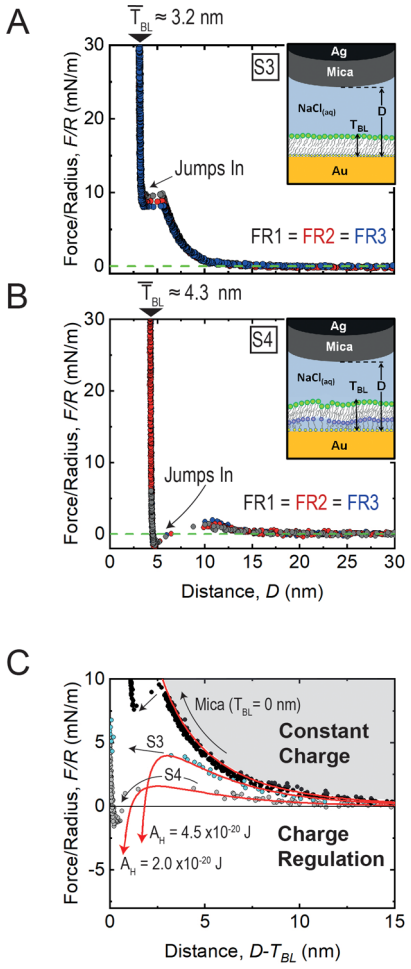

Figure 4. Force−distance curve profiles during the approach of SAM-based SLBs against mica. (A) Force runs (FRs) of system S3 (DPPC/C_{16}) deposited on gold facing a mica surface (schematic inset, top right). The force F/R is normalized by the curvature of the crossed-cylindrical surfaces. The averaged bilayer thickness measured is indicated by $\overline{T}_{BL}$. (B) Force runs (FRs) of system S4 (DPPC/DPhyTL) on gold (schematic inset, top right). (C) Fit of the interaction forces of two mica surfaces brought into contact (black markers), S4 system against mica (gray markers) and S3 system against mica (blue markers). The abscissa is the distance between the two outer faces of the surfaces taken in analysis. When no SLB is present, T_{BL} = 0 nm. The mica−mica curve is well-fitted by a constant charge solution of the DLVO function, while the SAM SLB systems are fitted with a charge regulation solution, obtaining two different Hamaker constants A_H and a Debye length λ_D = 3.70 ± 0.20 nm (see the text and Table S2 for more details).

contact from about D = 6.5 to D = 3.7 nm, and a further compression over about 0.5 nm before a final hard wall is reached. Second, the S3 system exhibits a perfect stability in terms of the hard wall thickness and reproducibility. In particular, we recorded a thickness (hard wall) at maximum compression of T_{BL} = 3.16 ± 0.06 nm during the first force run (FR1), T_{BL} = 3.17 ± 0.06 nm and T_{BL} = 3.14 ± 0.07 nm during the second and the third force runs (FR2 and FR3). The thickness of similar bilayer systems has been investigated in previous work using neutron reflectivity[36] and molecular dynamics simulations.[37] In those works, the thicknesses (T_{BL} = 4 ± 1 nm) are on average higher, with about 1 nm of the total thickness assigned to the hydrated headgroup. This difference is likely caused by the confinement and consequent dehydration of the headgroup after the jump into a strongly adhesive contact of the S3 system. Further, one can see that all force runs of a single experiment exhibit identical interaction force profiles during approach of the S3 system and a mica surface, indicating excellent reproducibility.

Figure 4B shows three consecutive force versus distance characteristics of the S4 system facing a mica surface. The profiles of the different approaches show the same shape, and they exhibit a defined jump-in from about D = 10 nm into D = 4.3 nm, which corresponds to the thickness of the bilayer model. In contrast to S3 the force profiles indicate a lower electric double layer repulsion followed by a jump into a slightly attractive regime and again a compression over about 0.5 nm into the repulsive hard wall.

At the maximum applied load the hard wall thickness of T_{BL} = 4.3 ± 0.5 nm for S4 was stable over more than 5 repeated runs. As for the S3 system, the hard wall in contact is about 1 nm lower compared to values for uncompressed and hydrated DPhyPC/DPhyTLs bilayer heights from neutron reflectivity studies[38] and in the expected range for a confined bilayer under applied load.[8,10,13,28] This is consistent with confinement effects in SFA such as interdigitation, headgroup dehydration, and polymer compression of the PEG4 tether in the present case. Moreover, this interpretation conforms with the AM-AFM measurements on S4: In Figure 3D the topography of the S4 bilayer shows undulations of the bilayer, which are derived from the soft properties of the polymer (polyethylene glycol, PEG) linker chains in the DPhyTL.

As shown in Figure 4C the measured equilibrium force versus distance characteristics during approach of systems S3 and S4 against the highly charged mica can be fitted well at distances $D - T_{BL} > 2-3$ nm as a linear superposition of electric double layer (F_{EDL}) and van der Waals (F_{VdW}) interactions using the DLVO theory. Here, these systems are highly asymmetric in terms of their electric double layer properties; hence, the electric double layer contribution is described using a charge regulation (CR) model for two asymmetric surfaces[39,40] as follows:

$$\frac{F_{DLVO}}{R} = \frac{F_{VDW}}{R} + \frac{F_{EDL}}{R} = -\frac{A}{6(D - D_{VdW})^2} + 2\pi\epsilon\epsilon_0\kappa \frac{[2\psi_1\psi_2 e^{-\kappa(D-D_{EDL})} + ((2p_1 - 1)\psi_2^2 + (2p_2 - 1)\psi_1^2)e^{-2\kappa(D-D_{EDL})}]}{1 - (2p_1 - 1)(2p_2 - 1)e^{-2\kappa(D-D_{EDL})}} \quad (1)$$

where ψ_n indicates the potential at the diffusive layer for each of the surfaces in a 1:1 electrolyte solution, ϵ and ϵ_0 are the electric permittivity of water and the permittivity of free space, A_H is the Hamaker constant, and κ is the inverse of the Debye length λ_D.[39,40] D_{EDL} and D_{VdW} describe the plane of origin of the individual force contributions. Specifically, for VDW contributions a shift of the plane of origin allows a simple modeling of layered systems, and EDL interactions originate from the diffuse layer interaction, which can hence be shifted by the thickness of the inner electric double layer.[41] The parameters p are charge regulation parameters and converge the interaction to the constant charge solution (CC) if p = 1 or to the constant potential solution (CP) if p = 0 for the respective surface. The principal plane of origin for the fitting is defined as the closest approach of the bilayer and mica, as $D_0 = D - T_{BL} = 0$. VDW or EDL shifts refer to this plane.

In our fitting approach we initially fitted parameters for the mica surface in a symmetric experiment to fix the parameter p

DOI: 10.1021/acs.langmuir.9b01942
Langmuir 2019, 35, 15552−15563

for mica; all fitting parameters are listed in the Supporting Information, Table S2. Hence, Figure 4C also shows the force distance characteristic measured across two approaching mica surfaces. The profile is highly repulsive during approach and shows a jump into a hard wall at about 1 nm. This is fully consistent with a constant charge behavior with the counterions remaining within the contact zone. The 1 nm hard wall agrees well with a hydrated sodium layer confined between the hydrated mica surfaces. As can be seen in Figure 4C, the data can be well-fitted with eq 1 using a charge regulation parameter of $p_1 = p_2 = p_{mica} = 0.9$ and a diffuse double layer potential located at $D_{EDL} = 0.5$ nm of $\psi_1 = \psi_2 = \psi_{mica} = -71 \pm 4$ mV, depending on the particular mica used. Hence, mica can be well-described in terms of a constant charge surface down to distances of about $D = \frac{1}{\kappa}$, as expected. At smaller distances hydration effects overpower the DLVO contribution across symmetric mica versus mica force versus distance characteristics, which are not fitted here.

With this set of mica parameters, we can consistently fit the force versus distance characteristics for both the S3 and S4 systems while approaching a mica surface. Both bilayer models are well-described by considerably lower charge regulation parameters. Specifically, the S3 and the S4 system are fitted well with $p = 0.4$ and $p = 0.35$, respectively. As such, these surfaces are characterized more closely by constant potential solutions. The diffuse layer potential of the S4 system is low at $\psi_{S4} = -27 \pm 2$ mV. Utilizing Grahame's equation this corresponds to a charge density of -0.03 C/m^2, or one charge per 700 nm^2. This is about one charge per 10 lipid head groups on the surface, suggesting a charging of the neutral lipid by anion, here chloride, adsorption.

The location of anions and cations at lipid/water interfaces is an ongoing discussion in the literature. Experiments[42,43] and simulations[44,45] usually focus on salt concentrations of 100 mM and above. The adsorption of chloride is found to occur weakly in the ordered (LC) phase without binding by Aroti et al.[42] The work of McLaughlin et al.[43] on the adsorption of divalent cations to PC lipids finds negative ζ potentials for the PC lipid in their background 100 mM NaCl electrolyte; these are both consistent with the weak charging that we observe, albeit in a lower-concentration NaCl electrolyte. Notably, the simulations find both coordination of the sodium ions deep into the headgroup regions and the chloride ions located between 0.5 and 1 nm away from the PC headgroup, causing the potential across the bilayer to change,[44] also consistent with our hypothesis. Additional ions, as contaminants from the Milli-Q water or the salt used, are at suitably low concentrations (see ICP-MS data in the Supporting Information, Table S1) that they will not have an influence on the surface charging.

Interestingly, the diffuse layer potential of the S3 system is considerably higher at $\psi_{S3} = -53 \pm 2$ mV, corresponding to a charge density of -0.058 C/m^2, or one charge per 275 nm^2. This indicates a considerably higher negative surface charging of the DPPC anchored to the SAM surface. This is consistent with an increased VDW attraction of the highly polarizable chloride ions to the surface, due to the substrate gold layer, which is located about 3 nm below the surface for the S3 case and more than 4.2 nm below the surface for the S4 case. This interpretation is also consistent with higher overall VDW interactions and a larger jump into contact distance observed for the S3 system (see again the fit in Figure 4C).

As already mentioned, at shorter separation distances below $D = 2-3$ nm the surfaces deviate from DLVO behavior, which is that they show an instability and jump-in to close contact, followed by a short-range repulsion over 0.5 nm. The instability at $D = 7-10$ nm seems to correlate with an overpowering of the electric double layer repulsion by attractive van der Waals interactions for the S3 and S4 systems, with a larger effective Hamaker constant of the S3 system. This agrees well with the thinner film thickness and hence larger contribution of the underlying gold substrate. For the S4 system the short-range repulsion can be fitted reasonably well with either of the following two models: First, a short-range exponential hydration repulsion with a quite short scaling length of 2–3 Å fits the data. Second, a $1/D^3$ dependence of a Helfrich-like model.[46] The former may relate to the headgroup dehydration, while the latter is related to an undulation repulsion. In Figure 5 we show a representative fit for both hydration states of the S4 system at distances where a short-range repulsion occurs just after the jump into contact. In blue, we show exponential decays for progressively thinner hydration scaling lengths from $\lambda_{Hy} = 1$ nm, which does not fit the data at all, through a typical hydration layer thickness ($\lambda_{Hy} = 0.3$ nm) to 0.15 nm, which, despite fitting the data, is a distance lower than any hydrated ion shell size. Thus, an exponential model does not properly describe the repulsion recorded with reasonable parameters. On the other hand, a Helfrich model[46] can fit very well all the data sets with a reasonable bending modulus $k_b = 2.5-5.0 \times 10^{-19}$ J, which is in line with previous results.[47] Therefore, after the jump-in occurs, and the PEG chains are compressed, the S4 SLB systems need time to relax the undulations that still persist at the bilayer interface, which can be well-described by the Helfrich model. On the basis of the current data we conclude that the short-range repulsion maybe a superposition of both contributions, while it seems evident that the repulsion

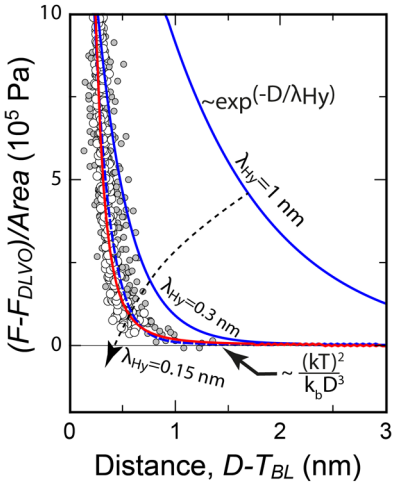

Figure 5. Helfrich and hydration pressure fit of S4 SLBs. Fit of representative force profiles of both fully hydrated (open circles) and not fully hydrated (full circles) S4 systems at short distances after the jump-in to contact occurred ($\ll 4$ nm). The force is normalized by subtraction of background DLVO interaction and by a nominal area ($\sim 100\ \mu m^2$), typical at these distances after jump-in. Presented in blue are the exponential fits (hydration model) and in red the Helfrich undulation model fit (cf. the text for details).

DOI: 10.1021/acs.langmuir.9b01942
Langmuir 2019, 35, 15552−15563

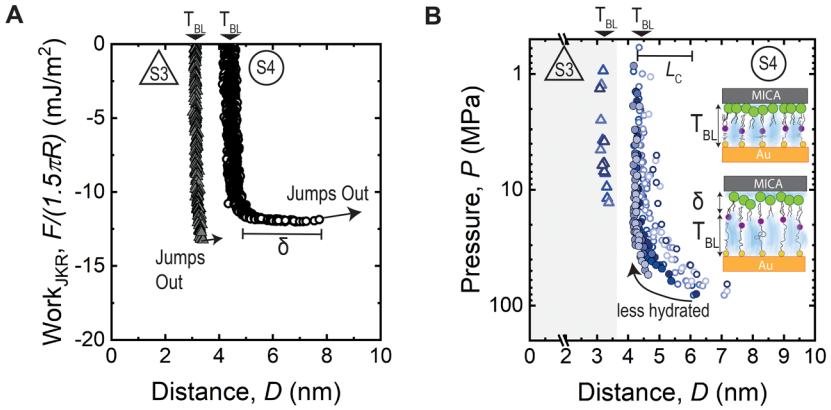

Figure 6. Adhesion and pressure for SAM-based systems. (A) Force profiles during surface separation for S3 (triangles) and S4 hydrated (open circles). Before each jump-out, the S4 system increases its thickness in confinement by a quantity δ while keeping the force constant. (B) Adhesive pressure measured as a function of the distance for S3 (triangles) and both S4 fully hydrated (open circles) and not fully hydrated (full circles) systems. The different runs are displayed with a graduated blue scale where the darkest is the first retraction. The contour length L_C of the PEG system is displayed for comparison with δ (see inset sketch). Note, the adhesive pressures have been made positive for the convenience of plotting on a logarithmic scale.

after the jump is dominated by the damping of the natural undulations of the systems.[48]

Figure 6 shows characteristic (A) force (normalized by 1.5πR) and (B) pressure versus distance profiles during separation for the two SAM-based bilayers, S3 and S4, from mica, respectively. [Pressure values were calculated from the force measured by the strain gauge divided by the area measured from the contact radius of the FECO at each of the points. For the contact diameter measurement a threshold difference of 15% from the distance at the center to the distance at the contact edge was used.] In Figure 6A the points where the adhesive junctions break and the surfaces suddenly jump apart to some large distance are marked as "Jumps Out". Interestingly, both systems show a considerably different contact geometry and force versus distance characteristic during separation, and the S4 system shows a pronounced dependence on the preparation history, as follows.

First, in Figure 6A the normalized force versus distance characteristics for the S3 system show a distinct jump-out from the bilayer thickness with a small 3−5 Å extension from the hard wall at higher pulling forces. The measured adhesive force of 62 ± 12 mN/m is stable over three consecutive force runs at the same position. This suggests that the S3-supported bilayer remains stable upon multiple separations under high adhesive load. The 3−5 Å extension may be due to increased undulations under high pulling forces, where they are not damped any longer, due to a change of the tilt angle during pulling, or due to rehydration of the headgroups just before adhesive separation. A potential rehydration will not have been observed in past bilayer versus bilayer studies, because the headgroups will remain hydrated at contact, because of the low adhesion and interaction energy of bilayers. A further alternative explanation would be that the increase in thickness is strain of the mica under the adhesive load; however, this is highly unlikely for the S3 system. [The maximum possible extension of mica in the elastic limit can be calculated from the elastic modulus, E, using $\Delta L = (FT_{mica})/(AE) = (1.2\ \text{mN} \times 6.3\ \mu\text{m})/(1000\ \mu\text{m}^2 \times \text{GPa}) = 0.08$ nm, from the lowest value of the mica E to 0.027 nm for the upper value of 180 GPa in the range. This is below the typical detection limit of SFA.] We may only further clarify the cause of the extension with an SFA/spectroscopy combination, as anticipated in ongoing work by this and other groups.

Quite in contrast, for the S4 system the force versus distance profiles display a pronounced gradual increase in the distance at constant force. This results in a plateau of constant force stretching a distance of approximately δ = 2.5 nm for the fully hydrated S4 and 1.3 ± 0.2 nm for the not fully hydrated S4 just before the surfaces jump apart. The stretching distance δ is hence 5−8 Å smaller, or 5−10 Å larger compared to the full contour length L_C = 1.5 nm of the PEG chain in the system, respectively, depending on the preconditioning (hydration). The L_C is a relevant length scale if polymer extension is the only active process during separation. Therefore, it is often taken as a reference for similar shapes observed for other tethered systems. Here, the extension is more complex and also depends on the preparation conditions, which will be discussed below (in the fourth paragraph).

S3 is hence acting as a rigid system without significant extension before contact separation, a property that comes from the rigid C_{16} structure, which is strongly bound to the substrate propagating its rigidity to the entire bilayer through the densely formed SAM. As such, the S3 system can be treated as a JKR contact, and the work of adhesion can be directly evaluated from Figure 6A. In contrast, the S4 system indicates an extension of the system's thickness while still in adhesive contact, with a pronounced L-shape of the force versus distance profiles. This is comparable to more gradual U-shaped profiles observed for soft adhesive systems containing PEG chains for ligand/receptor probing.[10] This is consistent with a stretching of the system (PEG4) before adhesive failure occurs. As a result, the work of adhesion cannot be evaluated using the JKR model, and the measured forces cannot be immediately compared to the S3 model system. The S4 data are put on the same axes in Figure 6A for ease of comparison only.

Second, and as shown in Figure 7, this behavior is also reflected in the contact geometry recorded in situ with the SFA during separation. FECO recorded at the point of separation indicates an extended flat contact for the S3 system, and the area versus applied load curve shows a typical JKR shape (analysis not shown). The adhesion is also independent of the load applied during approach (see the SI, Figure S4). However,

DOI: 10.1021/acs.langmuir.9b01942
Langmuir 2019, 35, 15552−15563

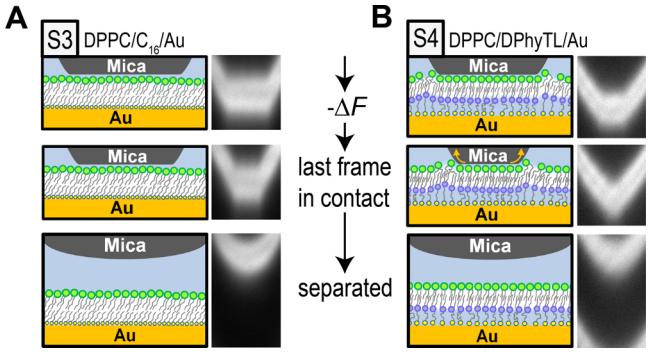

Figure 7. Jump-out events for systems S3 (A) and not fully hydrated S4 (B). System S3 has a slight decrease in contact area during the expansion but detaches from a relatively large contact area (more than 800 μm^2). The middle figure in part A shows the last FECO recorded before the jump-out event. (Note that all FECO, i.e., odd and even, show the same shape in this system. See the SI, Figure S2.) This behavior indicates that the system is well-described by the JKR model. In system S4, by comparison, we observed a rapid decrease in contact area before jumping out (less than 300 μm^2), indicating that the lipid molecules are constantly peeled off the mica surface before the complete detachment (indicated by the arrows in the middle figure of part B). This is due to the soft inner DPhyTL layer, giving the lipids more flexibility in the vertical direction.

the S4 system indicates a strongly decreasing contact area during separation and hence increasing pressure, which is not consistent with the separation of a JKR contact, yet appears consistent with a peel-off at constant force. This is due to additional modes of deformation originating from a soft and polymer-tethered bilayer architecture.

Third, Figure 6B shows the data for S4 and S3 in terms of pressure (force/area) versus distance characteristics and compares both systems in terms of the adhesive pressure during separation. The direct comparison of the adhesive pressures and forces during separation suggests that both systems, S3 and S4, reach comparable adhesive forces of F/R = 60−80 mN/m or W_{JKR} = 12−14 mJ/m^2 (see again Figure 6A,B), while adhesive pressures are, as expected, much higher in the S4 case that separates by a peel-off mechanism, where the contact area decreases at constant force. It is interesting to note that the distance for S4 increases roughly at the pressure level of 10−20 MPa where S3 separates completely, indicating a different detachment path and hence work.

Fourth, for S4, Figure 6B further shows representative pressure versus distance profiles during separation for two sets of 5 consecutive repetitions (filled and open round symbols). The two sets differ in their time of exposure to water after the DPhyTL monolayer preparation. Specifically, in initial experiments we LB-deposited the outer DPPC layer directly after drying the ethanol-washed DPhyTL monolayer following its deposition. In a second set of experiments the DPhyTL was allowed to rehydrate for >10 h in Milli-Q water, prior to DPPC deposition in the LB trough. While the adhesive pressure during separation reaches similar values of about 80−100 MPa, the shape of the pressure versus distance profiles shows distinctly different characteristics for the two preparation methods. Specifically, for the system with no additional hydration time the extension δ decreased significantly from 1.5 to 0.6 nm upon consecutive probing. However, it remained constant and about 0.5−1 nm above the full contour length of the PEG4 for the >10 h hydrated system.

The decreasing δ for systems with short hydration time during preparation indicates that DPhyTL in the bilayer architecture may dehydrate under continuous probing, if it is not preconditioned properly by extended hydration of the DPhyTL monolayer. This is consistent with an average hard wall decrease compared to the hydrated system that is within a few Å, yet close to the noise level.

For the hydrated system the observation of a plateau of constant force extending further than L_C is interesting and may be explained as follows. We do not observe any decrease in adhesive force or any change of the hard wall thickness with repeated probing. Thus, we cannot apply an explanation of lipid pluck-out that was observed in other systems with highly adhesive bonds,[11] where a decrease of the interaction force was observed upon consecutive force probing.

We find the thickness of the "stretched system" as it jumps out of contact is about 1−1.5 nm greater than that of its measured thickness under no applied load of about 5.8 nm (using neutron reflectivity[38]). As a word of caution, the last points during jump-out are separated by more than 4−6 Å from the previous point (at 10 Hz frame rate); it is hence not clear whether these points are to be considered as "still in contact" or "detached and flying apart". This makes any definition of a plateau length somewhat uncertain within the limit of the last two points recorded. Regardless, extending from the natural uncompressed height of 5.8 nm, an additional 1−1.2 nm of the maximum observed stretching can be explained by a rehydration of the maximum observed stretching of the headgroups (0.3 nm) and re-establishment of natural undulations during separation (0.3 nm) in combination with the hydrated PEG4 linker stretching from its natural Flory radius to full extension at L_C (0.6−0.8 nm). Any additional unaccounted extension may well be related to an elastic deformation (0.3 nm) of the entire mica crystal under the high adhesive pressure in this situation, and any linear combination of all four potential contributions is possible. [During a peel-off process the interaction area at separation decreases by 1 order of magnitude, so that, for an adhesive force of F = 1.2 mN, mica thickness T_{mica} = 6.3 μm, contact area at jump-out A = 100 μm^2, and an elastic modulus E in the range 90−180 GPa, a maximum elastic mica expansion of about 0.8 or 0.3 nm is estimated, respectively, with a higher E value more likely for the thick mica sheets used. In the case of a decreasing contact area mica expansion can hence play a role in establishing the observed longer de-adhesion plateaus.]

This interpretation is also consistent with the observed decrease of the plateau length for the nonhydrated DPhyTL system (Figure 6B, filled circles). That system shows an extension δ that decreases to 5−8 Å after consecutive probing. The decrease is consistent with the PEG extension that may become shorter and insignificant upon consecutive probing due to PEG4 dehydration or reordering, as the initial hydration state was different from the preconditioned, hydrated S4 (Figure 6B open circles). The final PEG4 behavior in the nonhydrated (not preconditioned) state is hence more equivalent to a polymer in a bad solvent. Hence, the remaining 5−8 Å total expansion may be consistent again with mica expansion, undulations, and headgroup rehydration as dominating factors in the dehydrated case after extensive probing.

Therefore, in any case the explanation for the extension of these systems is complex; δ must be a combination of the polymer stretch and the hydration of both the lipid headgroups

DOI: 10.1021/acs.langmuir.9b01942
Langmuir 2019, 35, 15552−15563

and the PEG4 itself, with potential contributions from elastic mica deformations, depending on the interactive area during separation. Compared to tethered ligand/receptor separation[11] this complex detachment mechanism may also explain the more pronounced L-shape of the separation, as compared to the gradual U-shape observed for ligand/receptor systems, which is due to the sequential unbinding at the outer rim of a gradually detaching contact.

In conclusion, it is interesting to compare the measured data, existing data, and simulation work on bilayers contacting solid surfaces. First, the observed adhesion is close to the adhesion observed during hemifusion of lipids by Benz et al.[13] and of hydrophobic surfactant monolayers by Helm et al.[2] but remains below the equivalent load (200 mN/m) that would be required to separate two fused bilayers.[49] As such, the hydrophobic attraction maintains the stability of the S3/S4 bilayer systems during separation, and the measured adhesion energy (JKR for S3) and adhesive pressure (for S4) are a good approximation for a DPPC/mica interaction, in rigid and soft support architectures, respectively.

Compared to the work of Anderson, where a DPPC bilayer was approaching a silica surface,[15] our data indicate a clear jump into an adhesive contact for all four systems, followed by a hydration/undulation repulsion during close approach and high adhesion during separation, for both the S3 and S4 systems. The main differences evolve from surface roughness, which is different between a silica surface and mica, changing the force profile and adhesion when an SLB is approached.[8,50] In the force profile, roughness asperities can cause the repulsion during the approach of the surfaces to decrease, followed by an earlier increase in the repulsion force than expected as the surfaces begin to make contact at a greater distance, and dependent on the substrate material, the asperities are compressed. Therefore, a well-defined attractive jump into contact is absent in a rough system such as silica used by Anderson et al.[15] In addition, compared to the DPPC system (S1) for a rough system, it is less likely to see similarly significant transfer of material and multilayer formation, due to the lower effective contact area and local high curvatures of asperities.[15]

Finally, the force profile and work of adhesion of the rigid system are very similar to profiles simulated by Pertsin and Grunze for a PC lipid.[51] While the simulation data also show a clear effect of undulation and protrusion interactions at small bilayer/mica separations below 1 nm leading to a jump into contact, we find that the jump into contact appears at a larger distance, which may relate to larger VDW forces (induced by the gold support) not present in simulations. Still in close contact we do see a compression over a distance of D = 0.5 nm, which appears to be consistent with undulations and possibly protrusions, while a dehydration contribution cannot be excluded at this point. Here, only simulation of this particular system and spectroscopy probe experiments may allow a more detailed molecular-level insight.

CONCLUSIONS

In this work, we explored different ways to reach good stability of SLBs in SFA experiments under highly adhesive conditions. To increase the stability under adhesive loads, we tested systems with different inner layers. Using a cationic lipid, DPTAP, to compensate some of the mica charge provided a layer free from holes in the AM-AFM measurements. This is a significant improvement over uncharged lipids, which led to some enhancement of stability. However, it was not sufficient under the high loads against mica to maintain a consistent thickness over multiple measurements. Still this is an optional stabilization for experiments at lower adhesive force/pressure, which may be evaluated individually for such experiments. In particular, the DPPC only and DPTAP/DPPC systems are likely to remain stable for some symmetric bilayer versus bilayer experiments. The SAM-based SLBs have both shown a good stability under high adhesion (F/R = 60−80 mN/m, or F/A = 80−100 MPa), which is represented by consistent thicknesses and force profiles over multiple measurements. The systems we have introduced compare reasonably well to simulations of related systems.[16] The C_{16}-supported DPPC (S3) in particular had a very low roughness (RMS = 0.18 nm) and consistent thickness and adhesion values. However, the surface charge was quite high due to attraction of anions to the interface.

DPhyTL SAM-supported DPPC has a low intrinsic surface charge and exhibits undulations on the order of 0.6−1.5 nm if surfaces are prepared without sufficient rehydration time. Hence, for the DPhyTL system a sufficient hydration time is required to fully hydrate the PEG4 chains used in the anchoring system. The fully hydrated DPhyTL-supported layer is a very close representation of a floating DPPC bilayer, with undulations and a characteristic bending modulus of $k_b = 2.5 \times 10^{-19}$ J in the range expected for a DPPC bilayer. At the same time it maintains the greater interaction, to both the support and the outer leaflet, that the support layer requires so that the outer DPPC layer remains stable under the high adhesion generated at the DPPC/mica interface. Both SAM-supported systems behave as constant charge surfaces. Both systems appear to charge negatively by anion adsorption while the C_{16} supported DPPC (S3) has a higher intrinsic surface charge, potentially due to higher van der Waals attraction of anions to the interface.

In summary, SFA measurements provide unique distance-dependent interaction profiles enabling molecular-scale insight into the forming and breaking of adhesive bonds of four different bilayer model systems. Specifically the DPhyTL-based system offers diverse possibilities for new applications in SFA, including the operando combination of SFA during bond forming and breaking in biomimetic systems with bio- and electrochemical sensing, where DPhyTL membranes are state of the art, providing excellent electrochemical membrane characteristics (see also impedance in the SI, Figure S5).

ASSOCIATED CONTENT

Supporting Information

The Supporting Information is available free of charge on the ACS Publications website at DOI: 10.1021/acs.langmuir.9b01942.

Water quality data, surface-pressure isotherms for DPPC and DPTAP, FECO, AFM topographies, plots of the adhesion force, DLVO fitting parameters, and impedance spectroscopy (PDF)

AUTHOR INFORMATION

Corresponding Author

*E-mail: valtiner@iap.tuwien.ac.at.

ORCID

Pierluigi Bilotto: 0000-0001-6531-8528

Laura L. E. Mears: 0000-0001-7558-9399

DOI: 10.1021/acs.langmuir.9b01942
Langmuir 2019, 35, 15552−15563

Markus Valtiner: 0000-0001-5410-1067

Author Contributions

[‖]P.B. and M.L. contributed equally to this work. M.V., L.L.E.M., M.L., and P.B. planned, discussed, interpreted, and conducted research and wrote the manuscript jointly. J.A. assisted with the preparation of DPhyTL membranes, discussed and interpreted results, and coprepared the manuscript. U.R. joined the project at a late stage, performed the impedance measurements for the DPhyTL-based bilayer systems, and discussed the research and manuscript.

Notes

The authors declare no competing financial interest.

■ ACKNOWLEDGMENTS

P.B., M.L., U.R, L.L.E.M. and M.V. acknowledge support by the European Research Council (Grant: CSI.interface, ERC-StG 677663). Max-Planck Institut für Eisenforschung as well as the Austrian Institute of Technology (Biosensor lab in Tulln, AT) are thanked for providing access to physical vapor deposition. We are grateful to Dominik Dworschak for sharing the ICP-MS data of water. We would also like to thank Wolfgang Knoll for suggesting the DPhyTL system to us. U.R. was also partly supported by the Competence Center for Electrochemical Surface Technology (CEST) in the framework of the COMET scheme of the Austrian Research Promotion Agency (FFG, project 865864). This paper is dedicated to Jacob N. Israelachvili, who pioneered SFA and inspired membrane studies with the SFA.

■ REFERENCES

(1) Helm, C. A.; Knoll, W.; Israelachvili, J. N. Measurement of ligand-receptor interactions. *Proc. Natl. Acad. Sci. U. S. A.* **1991**, *88*, 8169−8173.

(2) Helm, C. A.; Israelachvili, J. N.; McGuiggan, P. M. Molecular Mechanisms and Forces Involved in the Adhesion and Fusion of Amphiphilic Bilayers. *Science* **1989**, *246*, 919−922.

(3) Prakasam, A. K.; Maruthamuthu, V.; Leckband, D. E. Similarities between heterophilic and homophilic cadherin adhesion. *Proc. Natl. Acad. Sci. U. S. A.* **2006**, *103*, 15434−15439.

(4) Shi, Q.; Maruthamuthu, V.; Li, F.; Leckband, D. Allosteric Cross Talk between Cadherin Extracellular Domains. *Biophys. J.* **2010**, *99*, 95−104.

(5) Marra, J.; Israelachvili, J. Direct Measurements of Forces between Phosphatidylcholine and Phosphatidylethanolamine Bilayers in Aqueous Electrolyte Solutions. *Biochemistry* **1985**, *24*, 4608−4618.

(6) Israelachvili, J. N.; Wennerström, H. Entropic forces between amphiphilic surfaces in liquids. *J. Phys. Chem.* **1992**, *96*, 520−531.

(7) Helm, C. A.; Israelachvili, J. N. Forces between Phospholipid Bilayers and Relationship to Membrane Fusion. *Methods Enzymol.* **1993**, *220*, 130−143.

(8) Orozco-Alcaraz, R.; Kuhl, T. L. Interaction Forces between DPPC Bilayers on Glass. *Langmuir* **2013**, *29*, 337−343.

(9) Lee, D. W.; Kristiansen, K.; Donaldson, S. H.; Cadirov, N.; Banquy, X.; Israelachvili, J. N. Real-time intermembrane force measurements and imaging of lipid domain morphology during hemifusion. *Nat. Commun.* **2015**, *6*, 7238.

(10) Kuhl, T. L.; Leckband, D. E.; Lasic, D. D.; Israelachvili, J. N. Modulation of interaction forces between bilayers exposing short-chained ethylene oxide headgroups. *Biophys. J.* **1994**, *66*, 1479−1488.

(11) Kuhl, T.; Guo, Y.; Alderfer, J. L.; Berman, A. D.; Leckband, D.; Israelachvili, J.; Hui, S. W. Direct Measurement of Polyethylene Glycol Induced Depletion Attraction between Lipid Bilayers. *Langmuir* **1996**, *12*, 3003−3014.

(12) Valtiner, M.; Donaldson, S. H.; Gebbie, M. A.; Israelachvili, J. N. Hydrophobic Forces, Electrostatic Steering, and Acid−Base Bridging between Atomically Smooth Self-Assembled Monolayers and End-Functionalized PEGolated Lipid Bilayers. *J. Am. Chem. Soc.* **2012**, *134*, 1746−1753.

(13) Benz, M.; Gutsmann, T.; Chen, N.; Tadmor, R.; Israelachvili, J. N. Correlation of AFM and SFA Measurements Concerning the Stability of Supported Lipid Bilayers. *Biophys. J.* **2004**, *86*, 870.

(14) Andersson, J.; Köper, I. Tethered and Polymer Supported Bilayer Lipid Membranes: Structure and Function. *Membranes* **2016**, *6*, 30.

(15) Anderson, T. H.; Min, Y.; Weirich, K. L.; Zeng, H.; Fygenson, D.; Israelachvili, J. N. Formation of supported bilayers on silica substrates. *Langmuir* **2009**, *25*, 6997−7005.

(16) Pertsin, A.; Grunze, M. Possible mechanism of adhesion in a mica supported phospholipid bilayer. *J. Chem. Phys.* **2014**, *140*, 184707.

(17) Atanasov, V.; Knorr, N.; Duran, R. S.; Ingebrandt, S.; Offenhausser, A.; Knoll, W.; Koeper, I. Membrane on a Chip: A Functional Tethered Lipid Bilayer Membrane on Silicon Oxide Surfaces. *Biophys. J.* **2005**, *89*, 1780−1788.

(18) Vockenroth, I. K.; Atanasova, P. P.; Jenkins, T. A.; Koeper, I. Incorporation of α-Hemolysin in Different Tethered Bilayer Lipid Membrane Architectures. *Langmuir* **2008**, *24*, 496−502.

(19) Andersson, J.; Knobloch, J.; Perkins, M.; Holt, S.; Koeper, I. Synthesis and Characterization of Novel Anchorlipids for Tethered Bilayer Lipid Membranes. *Langmuir* **2017**, *33*, 4444−4451.

(20) Goreham, R.; Thompson, V.; Samura, Y.; Gibson, C.; Shapter, J.; Koeper, I. Interaction of Silver Nanoparticles with Tethered Bilayer Lipid Membranes. *Langmuir* **2015**, *31*, 5868−5874.

(21) Andersson, J.; Fuller, M.; Holt, S.; Koeper, I. A tethered bilayer lipid membrane that mimics microbial membranes. *Phys. Chem. Chem. Phys.* **2018**, *20*, 12958−12969.

(22) Knoll, W. *Private Communication*, 2018.

(23) Junghans, A.; Köper, I. Structural Analysis of Tethered Bilayer Lipid Membranes. *Langmuir* **2010**, *26*, 11035−11040.

(24) Zhang, G.; Wei, Z.; Ferrell, R. E. Elastic modulus and hardness of muscovite and rectorite determined by nanoindentation. *Appl. Clay Sci.* **2009**, *43*, 271−281.

(25) Chen, Y. L.; Helm, C. A.; Israelachvili, J. N. Measurements of the elastic properties of surfactant and lipid monolayers. *Langmuir* **1991**, *7*, 2694−2699.

(26) Schwenzfeier, K. A.; Erbe, A.; Bilotto, P.; Lengauer, M.; Merola, C.; Cheng, H.; Mears, L. L. E.; Valtiner, M. Optimizing multiple beam interferometry in the surface forces apparatus: Novel optics, reflection mode modeling, metal layer thicknesses, birefringence, and rotation of anisotropic layers. *Rev. Sci. Instrum.* **2019**, *90*, 043908.

(27) Israelachvili, J. Recent advances in the surface forces apparatus (SFA) technique. *Rep. Prog. Phys.* **2010**, *73*, 036601.

(28) Rand, R.; Parsegian, V. Hydration forces between phospholipid bilayers. *Biochim. Biophys. Acta, Rev. Biomembr.* **1989**, *988*, 351−376.

(29) Wong, J. Y.; Kuhl, T. L.; Israelachvili, J. N.; Mullah, N.; Zalipsky, S. Direct Measurement of a Tethered Ligand-Receptor Interaction Potential. *Science* **1997**, *275*, 820−822.

(30) Khan, M. S.; Dosoky, N. S.; Williams, J. D. Engineering Lipid Bilayer Membranes for Protein Studies. *Int. J. Mol. Sci.* **2013**, *14*, 21561.

(31) Hui, S.; Viswanathan, R.; Zasadzinski, J.; Israelachvili, J. The structure and stability of phospholipid bilayers by atomic force microscopy. *Biophys. J.* **1995**, *68*, 171−178.

(32) Armstrong, C. L.; Barrett, M. A.; Toppozini, L.; Kučerka, N.; Yamani, Z.; Katsaras, J.; Fragneto, G.; Rheinstädter, M. C. Co-existence of gel and fluid lipid domains in single-component phospholipid membranes. *Soft Matter* **2012**, *8*, 4687−4694.

(33) Gzyl-Malcher, B.; Filek, M.; Brezesinski, G. Mixed DPPC/DPTAP Monolayers at the Air/Water Interface: Influence of Indolilo-3-acetic Acid and Selenate Ions on the Monolayer Morphology. *Langmuir* **2011**, *27*, 10886−10893.

(34) Fréchette, J.; Kyle Vanderlick, T. Double layer forces over large potential ranges as measured in an electrochemical surface forces apparatus. *Langmuir* **2001**, *17*, 7620−7627.

DOI: 10.1021/acs.langmuir.9b01942
Langmuir 2019, 35, 15552−15563

(35) Valtiner, M.; Banquy, X.; Kristiansen, K.; Greene, G. W.; Israelachvili, J. N. The Electrochemical Surface Forces Apparatus: The Effect of Surface Roughness, Electrostatic Surface Potentials, and Anodic Oxide Growth on Interaction Forces, and Friction between Dissimilar Surfaces in Aqueous Solutions. *Langmuir* **2012**, *28*, 13080−13093.
(36) Meuse, C.; Krueger, S.; Majkrzak, C.; Dura, J.; Fu, J.; Connor, J.; Plant, A. Hybrid bilayer membranes in air and water:infrared spectroscopy and neutron reflectivity studies. *Biophys. J.* **1998**, *74* (3), 1388.
(37) Tarek, M.; Tu, K.; Klein, M.; Tobias, D. Molecular Dynamics Simulations of Supported Phospholipid/Alkanethiol Bilayer on a Gold (111) Surface. *Biophys. J.* **1999**, *77* (2), 964.
(38) Braunagel, J.; Junghans, A.; Koeper, I. Membrane-based Sensing Approaches. *Aust. J. Chem.* **2011**, *64* (1), 54.
(39) Popa, I.; Sinha, P.; Finessi, M.; Maroni, P.; Papastavrou, G.; Borkovec, M. Importance of Charge Regulation in Attractive Double-Layer Forces between Dissimilar Surfaces. *Phys. Rev. Lett.* **2010**, *104*, 228301.
(40) Carnie, S. L.; Chan, D. Y. C. Interaction free energy between plates with charge regulation: A linearized model. *J. Colloid Interface Sci.* **1993**, *161*, 260.
(41) Valtiner, M.; Kristiansen, K.; Greene, G. W.; Israelachvili, J. N. Effect of Surface Roughness and Electrostatic Surface Potentials on Forces Between Dissimilar Surfaces in Aqueous Solution. *Adv. Mater.* **2011**, *23*, 2294−2299.
(42) Aroti, A.; Leontidis, E.; Maltseva, E.; Brezesinski, G. Effects of Hofmeister Anions on DPPC Langmuir Monolayers at the Air-Water Interface. *J. Phys. Chem. B* **2004**, *108*, 15238−15245.
(43) McLaughlin, A.; Grathwohl, C.; McLaughlin, S. The adsorption of divalent cations to phosphatidylcholine bilayer membranes. *Biochim. Biophys. Acta, Biomembr.* **1978**, *513*, 338−357.
(44) Gurtovenko, A. A. Asymmetry of lipid bilayers induced by monovalent salt: Atomistic molecular-dynamics study. *J. Chem. Phys.* **2005**, *122*, 244902.
(45) Cordomí, A.; Edholm, O.; Perez, J. J. Effect of Force Field Parameters on Sodium and Potassium Ion Binding to Dipalmitoyl Phosphatidylcholine Bilayers. *J. Chem. Theory Comput.* **2009**, *5*, 2125−2134.
(46) Helfrich, W. Elastic Properties of Lipid Bilayers: Theory and Possible Experiments. *Z. Naturforsch., C: J. Biosci.* **1973**, *28*, 693−703.
(47) Nagao, M.; Kelley, E.; Ashkar, R.; Bradbury, R.; Butler, P. Probing Elastic and Viscous Properties of Phospholipid Bilayers Using Neutron Spin Echo Spectroscopy. *J. Phys. Chem. Lett.* **2017**, *8*, 4679−4684.
(48) Israelachvili, J. N. *Intermolecular and Surface Forces*, 3rd ed.; Academic Press, 2011.
(49) Helm, C. A.; Israelachvili, J. N.; McGuiggan, P. M. Role of Hydrophobic Forces in Bilayer Adhesion and Fusion. *Biochemistry* **1992**, *31*, 1794−1805.
(50) Donaldson, S. H.; Valtiner, M.; Gebbie, M. A.; Harada, J.; Israelachvili, J. N. Interactions and visualization of bio-mimetic membrane detachment at smooth and nano-rough gold electrode surfaces. *Soft Matter* **2013**, *9*, 5231.
(51) Pertsin, A.; Grunze, M. Computer simulations of water-mediated force between phospholipid membranes. *Curr. Opin. Colloid Interface Sci.* **2011**, *16*, 534−541.

DOI: 10.1021/acs.langmuir.9b01942
Langmuir 2019, 35, 15552−15563